Improving Needleless Electrospinning Throughput by Tailoring Polyurethane Solution Properties with Polysiloxane Additives

Kamran Iranshahi[1,2], Jean Schoeller[1,3], Nicolas Luisier[1], Michael Chung[4], Sina Hashemizadeh[5], Giuseppino Fortunato[1], Thijs Defraeye[1], René M. Rossi[1,3*]

[1]Empa, Swiss Federal Laboratories for Materials Science and Technology, Laboratory for Biomimetic Membranes and Textiles, Lerchenfeldstrasse 5, CH-9014 St. Gallen, Switzerland

[2]ETH Zürich, Department of Environmental Systems Science, 8092 Zürich, Switzerland

[3]ETH Zürich, Department of Health Science and Technology, 8092 Zürich, Switzerland

[4]School of Engineering, The University of Edinburgh, King's Buildings, Mayfield Road, Edinburgh EH9 3JL, United Kingdom

[5]Foundation for Research on Information Technologies in Society (IT'IS), Zeughausstrasse 43, CH-8004 Zurich, Switzerland

** Corresponding author's email: Rene.Rossi@empa.ch*

Abstract

Within the manufacturing industry, production velocity plays a key role with respect to economic turn-over rates. This issue is often a pivotal factor in the incorporation of developing technologies. For electrostatic spinning, which is based on the formation of nanoscopic fibrous elements and relatively low fiber throughput values, an increase is highly desirable for application at both laboratory and industrial scales. In this paper, a joint experimental-theoretical study is conducted to explore the impact of the solution properties on improving the electrospinning throughput. The needleless electrospinning process was selected due to its increased production rate and higher upscaling potential than other electrospinning approaches. Polyurethane solutions using polysiloxane additives were used as spinning solutions. The results show that additives, such as PDMS-OH, that decrease the solution surface tension and increase the solution viscosity can significantly improve the production rate of nanofibrous scaffolds. Our experiment shows that with as low as 2% w/w additive, the membrane weight increased from 0.99 to 5.55 56 g/cm^2. As such, the use of additives is beneficial for high throughput since surface tension, viscosity, and relative permittivity can be tailored to increase the electrospinning throughput. This study provides a stepping stone towards higher electrospinning throughput by tailoring solution properties with additives.

Keywords

Wire-based electrospinning, Nanofibers, DMF-based solution, Industrial scaling, Productivity, Modeling

This document is the accepted manuscript version of the following article:
Iranshahi, K., Schoeller, J., Luisier, N., Chung, M., Hashemizadeh, S., Fortunato, G., … Rossi, R. M. (2022). Improving needleless electrospinning throughput by tailoring polyurethane solution properties with polysiloxane additives. ACS Applied Polymer Materials. https://doi.org/10.1021/acsapm.2c00263

1. Introduction

Academic and industrial research on electrospinning and respective nanofiber properties is an area of rising interest, as seen in the continuously growing number of research publications and patents, including the broadening range of applications such as tissue engineering, drug delivery, sensors, or apparel[1–3]. Besides needle-based electrospinning approaches representing the most prominent technology, jet initiation and fiber spinning using wires, rotating disks, drums and coils, structured surfaces, bubbles by gas injection, rotary jets, and many others have also been demonstrated[4,5]. Wire-based (or so-called needleless) electrospinning technology is an effective processing method that can fabricate amounts of nanofiber membranes at an industrial scale. In this process, a high voltage difference, typically in the range of 30 to 80 kV, is applied between two wires. A tailored polymeric spinning solution continuously coats the emitter wire that is usually connected to the positive high voltage (Figure 1). The presence of a high electric field forms multiple cone-jet structures (i.e., Taylor cones) on the wire[6]. During jetting, drawing and drying processes take place by which the solution is pulled towards a counter electrode at the opposite charge in two subsequent modes of stable and unstable (whipping) modes. The latter mode incorporates a chaotic motion of the jet based on electrohydrodynamic principles and results in the formation of nonwoven membranes with randomly oriented nanofibers.

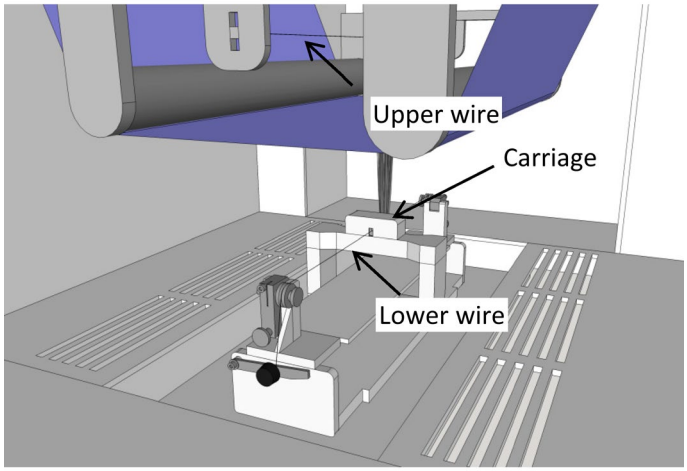

Figure 1 Scheme of the spinning chamber of the Nanospider™. Reprinted and adapted with permission from Döpke *et al.*[7]

Many studies have focused on tailoring fiber morphologies with respect to fiber diameter, homogeneity, orientation, and surface texture[8,9]. Spinning solution properties, environmental conditions, and electrospinning process parameters have been under investigation and optimization by scientists from the field. Regarding the solution parameters, it was revealed that polymer molecular weight, viscosity, electrical conductivity, and surface tension are critical factors in the fiber formation process and respective fiber properties [10–13]. Regarding the environmental conditions, both humidity and temperature have to be considered as they affect properties such as fiber diameters and surface texture[14–16]. Moreover, different process parameters like applied voltage, electrode gap as well as the spinning electrode and collector geometry have been examined for homogenous fiber formation[17,18].

As mentioned in the review articles by Xue et al.[19] and Luo et al. [20], the lack of research on process upscaling led to a gap between laboratory-scale research and industrial applicability. Not much knowledge is present with respect to investigations and the increase of the spinning throughput. Here, the term throughput refers to the amount of fiber material that can be produced by spinning per time unit. Although a study by Cengiz and Jirsak in 2009[21] demonstrated the influence of tetraethylammonium bromide (TEAB) salt on the electrospinning performance of polyurethane, the majority of work so far has involved changing the electrode geometry as a means to modulate the number of jet formation and hence the throughput. Conventional single nozzle electrospinning typically reveals yields lower than

0.2 g/h[22], which is too low to meet industry demand. Using a multiple nozzle setup, a Korean company has been able to increase the production rate to ~6.5 g/h for nylon fibers [23]. In another example, a company in China could increase the productivity up to ~2000 m^2 per day electrospun PI nanofibrous mats/nonwovens in a single production line[24]. Despite all recent advances, the electrospinning technology is still facing challenges and issues, such as potential nozzle clogging or inter-jet perturbations limiting the spinneret density.

The present study aimed to investigate and enhance the spinning throughput using a wire-based electrospinning technology by tailoring the spinning solution properties while keeping constant spinning parameter conditions to obtain homogenous fiber morphologies within similar dimensions. Properties such as the solution rheology, electrical conductivity, and surface tension were investigated and correlated to the specific weights of the membranes. Surfactant additives with defined chemistry were introduced in low concentration ranges to study their effects on spinning solution properties and interaction with the wire electrode to finally target and improve the spinning throughput. Fibers and membranes were analyzed in terms of morphology, surface properties, and wettability. Mathematical models and physics-based computational simulations were used to deepen our understanding and gain more insight into the underlying physics of the process. The employed theoretical approach is beneficial to further explore the complex mechanisms that are difficult to fully explain experimentally. The model sheds light on the contributing factors within the electrospinning process and clarifies their impact on the spinning throughput. Consequently, the results of this joint experimental-theoretical approach demonstrate which process parameters should be targeted to further optimize the process toward upscaling and obtaining higher fiber production rates.

2. Experimental

2.1. Materials

N,*N*-dimethylformamide (DMF, ≥99.5%) was purchased from VWR. Polyurethane (PUR Elastollan C95A55, Mw: ~85'000 Da) was obtained from BASF. Tetraethylammonium bromide (TEAB, reagent grade, 98%), hydroxyl-terminated poly(dimethylsiloxane) (PDMS-OH, ~65 cSt and ~2550-3570 cSt), hydride-terminated poly(dimethylsiloxane) (PDMS-H, Mn: ~580), octamethyltrisiloxane (Mw: 236.53) and trimethylsilyl-terminated poly(methylhydrosiloxane) (PDMS-HCH_3, Mn: ~390) were purchased from Sigma-Aldrich and used without further purification. The molecular weight was measured using the gas permeation chromatography (GPC) method. The average molecular weight was 279 g.mol-1, and the polydispersity index was 1.02 (See Figure S1 of the supporting information file).

2.2. Electrospinning solutions preparation

All solutions were prepared by first dissolving PUR in DMF (14.5 % w/v) over three days on an overhead shaker. After clear solutions were obtained, the different additives (PDMS-OH, PDMS-H, PDMS-HCH_3, octamethyltrisiloxane, or TEAB) were added in desired concentrations and the solutions were further shaken until used for electrospinning or characterization. The amounts of additives were calculated in weight percent with respect to the polyurethane mass.

2.3. Electrospinning parameters

Electrospun membranes were obtained using a needleless instrument from Elmarco (Nanospider, NS 1WS500U) equipped with steel wire electrodes. The electric potential was set up to +60 kV on the spinning electrode and -10 kV on the counter electrode, with a distance of 250 mm. Collecting substrate rewinding speed was fixed constant to 18

mm/min, electrode wire speed to 60 mm/min and the solution bearing carriage coated the electrode with a speed of 150 mm/s.

Relative humidity and air temperature were controlled to 20 % and 22 °C, respectively, using a ML270 dehumidifier (Munters) combined with a NA2005 temperature and humidity controller (Munters). The airflow entering the Nanospider was set to 90 m^3/h and outflow to 105 m^3/h to ensure evaporation and evacuation of the solvent.

2.4. Solutions characterization

Electrical conductivity was determined using a Mettler Toledo SevenCompact S213 conductimeter equipped with an InLab 741-ISM probe. Rheological solution and emulsion properties were determined on a rheometer (Anton Paar Physica MCR 300, Austria) equipped with a cone–plate geometry. The system was applied in a controlled shear rate mode to assess the shear viscosities as a function of the shear rate. Flow curves with shear rates varying from 0.01–100 1/s were recorded at 22 °C. Average values for each solution were calculated from at least three measurements. Frequency scans were measured at 10% amplitude in a frequency range of 0.05 – 500 1/s at 22°C to assess complex viscosity, storage, and loss modulus. The zero-shear viscosity (η_0) was calculated from the flow curves using the Carreau-Yasuda approximation through the Rheoplus software (Anton-Paar, Switzerland).

Surface tension and contact angle to steel were measured using a drop shape analyzer (Krüss, DSA25). For the surface tension, 1.8 mm external diameter needles (NE45 Krüss) were used and pendent drops of 4.5 µL were analyzed. For the contact angle to steel, drops of 4 µL of the spinning solutions were deposited on the steel plate and left until they reached an equilibrium shape. The respective algorithms of the built-in software were used for the computations of surface tension and contact angle, respectively. Given results are the averaged values of triplicates.

The dielectric spectroscopy was performed with the DAK 3.5 probe system (Schmid & Partner Engineering AG (SPEAG), Switzerland) connected to a ZVA 67 (Rohde & Schwarz, Germany) vector network analyzer (VNA) covering the frequency range from 200 MHz–20 GHz. The DAK 3.5 is based on the high-precision open coaxial probe (OCP) with an outer/inner diameter of 3.5 mm / 0.93 mm, respectively, and an optimized and advanced solver. The probe was calibrated prior to each measuring session using the standard 3-point, Open, Short, and Load (de-ionized) calibration[25,26]. The uncertainties of the measurement were established according to [27] that includes possible systematic errors due to design, calibration uncertainties, temperature differences between the calibration and measurements, and VNA noise.

2.5. Membranes characterization

Electrospinning throughput was determined as follows: membranes were cut using a punching machine (SAMCO SB-25) and then weighed on a microbalance (Mettler Toledo AT261). The results given are the averaged values of triplicates. Scanning electron micrographs were recorded on a Hitachi S-4800 (Hitachi High-Technologies, Canada) at an accelerating voltage of 2 kV and a current flow of 10 µA. In order to reduce charging effects, mats were sputter-coated with 7 nm of Au/Pd (Polaron Equipment, SEM coating Unit E5100, Kontron AG, Switzerland) before imaging. Mean fiber diameters were determined from 100 individual measurements taken within representative microscopic fields using ImageJ software 1.51j8 (National Institutes of Health, USA). The water contact angles of the electrospun membrane were measured using a drop shape analyzer (Krüss, DSA25) and the respective built-in algorithm. Given results are the averaged values of triplicates.

Chemical surface composition was analyzed by X-ray photospectroscopy (XPS) on a PHI 5000 VersaProbe II instrument (USA) with a monochromatic AlKα X-ray source. The energy resolution of the spectrometer was set to 0.8 eV/step at a pass-energy of 187.85 eV for survey scans and 0.125 eV/step and 29.35 eV pass-energy for high-resolution region scans,

respectively. Charge effects were compensated by calibrating the C1s peak to 284.5 eV. Elemental compositions were determined using instrument-dependent atom sensitivity factors. The photoelectron-transitions C1s, O1s, N1s, and Si2p were selected to determine the elemental concentrations and the chemical shifts within the region scans. Data analysis and peak fitting were performed using CasaXP software (Casa Software Ltd, United Kingdom).

2.6. Jet density calculations

The impact of the additives on the jet density (i.e., number of jets per unit length of wire) was investigated experimentally to validate the theoretical model. To this end, videos of the electrospinning process in the instrument chamber were recorded. The frame timer was started at the moment the coating-wagon left the frame. Fifteen pictures with each one at a frame time of 500 ms were considered for the selected additives. In addition, the number of the jets was counted in a specific wire length and the distribution was statistically investigated. Selected pictures for all tests are available in the supporting information file.

2.7. Statistical analysis

Results are displayed as mean ± standard deviation. Statistical significance was assessed by a two-sided, non-paired student's t-test, and results were accepted as significantly different for $p < 0.05$. All the tests were performed in R[28].

3. Mathematical model

The mathematical expressions of different parameters (i.e., solution properties) that could affect the throughput are presented in this section. Due to the complexity of the coupled system of Navier-Stokes, Maxwell's, and conservation of energy equations, the throughput cannot be defined by a simple equation that can be solved analytically [29,30]. Nevertheless, with simplified mathematical models, it is possible to identify the parameters that affect the throughput of the electrospinning process. Despite their simplicity, these models provide an in-depth insight into the physical understanding of the complex phenomena associated with the impact of the different additives on the throughput, which could not be fully explained experimentally. The results of this analytical evaluation are thus useful for investigating the impact of the contributing factors toward increasing the production rate.

In this regard, the impact of solution properties (e.g., viscosity, density, dielectric permittivity, liquid-air surface tension, etc.) on the solution entrainment on the wire electrode, the cone-jet formation process, and the electrospinning throughput are evaluated by employing a joint analytical, experimental, and simulation method. This includes mathematically calculating the average solution film thickness and mass on the wire, counting experimentally and mathematically the number of jets, and performing dimensional analysis on the diameter and velocity of the jets. The employed model consists of equations for mass, momentum, and charge conservation. Electric field equations were developed based on electrostatic laws.

3.1. Amount of deposited solution on the wire electrode

At low Reynolds number, $Re = \frac{2r_{wire}\rho V}{\eta} < 1$, the amount of the deposited solution on the wire electrode is a function of two dimensionless numbers, namely the capillary number (Ca) and Bond number (Bo)[6] ;

$$Ca = \frac{\eta V}{\gamma} \quad (1)$$

$$Bo = \frac{\rho g r_{wire}^2}{\gamma} \quad (2)$$

where η (Pa.s), γ (N/m), V (m/s), r_{wire} (m), g (m/s^2), and ρ (kg/m^3) are the liquid viscosity, surface tension, coating velocity, electrode wire radius, gravity acceleration, and the solution density, respectively. These two numbers measure the viscous and gravitational forces relative to the surface forces, which are the three important forces for liquid entrainment (Figure 2). It has been demonstrated that liquid entrainment at low Re is strongly controlled by the capillary number and weakly dependent on the Bond number [6].

The capillary number in our study is large ($Ca > 10$), and it has been shown that for high capillary numbers ($Ca > 1$), the deposited solution thickness (h) becomes almost constant ($h \cong 0.34\, r_{wire}$ [31]) for coating a solid by drawing it out of a bath of liquid (i.e., unlimited entrainment flow rate). We use this criterion as the threshold of the maximum possible deposited solution thickness on the wire. However, for a laminar falling film flow with a limited flow rate of the solution released by the carriage on the wire, the following formula is used [32]:

$$h_\theta = \left(\frac{3\,\dot{m}\,\eta}{g\,\rho^2 \sin\theta}\right) \quad \text{and} \quad h = average(h_\theta) \quad (3)$$

where $\dot{m}$ (kg/s) is the maximum flow rate of the solution released by the carriage on the wire, and θ is the angular position around the wire, measured from the upper stagnation point (12 o'clock) on the wire. Note that evaporation was neglected because DMF is a low volatile liquid at room temperature (it has low vapor pressure (516 Pa) at room temperature).

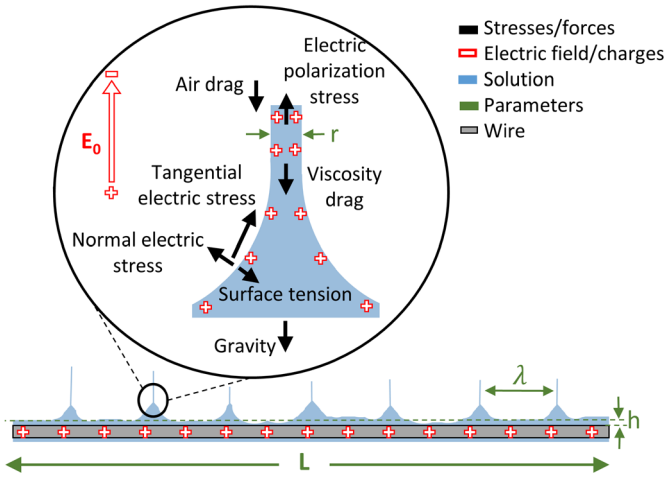

Figure 2 Schematic illustration of cone-jet formation on the wire electrode together with the main forces acting on the solution. (not to scale)

3.2. Mass flow rate and number of the jets

The mass flow rate of the jets can be calculated by using the conservation of mass equation and considering the jets as a one-dimensional flow (Eq. (4)).

$$Q = n\pi r_j^2 u\rho \quad (4)$$

Where Q (kg/s) is the mass flow rate, n is the calculated number of the jets on the wire, r_j (m) is the average radius of the jets (see Figure 2), u (m/s) is the average jet velocity, and ρ (kg/m^3) is the density of the solution. The number of jets (n) was calculated using the formula provided in [33,34] for needleless electrospinning.

$$n = \frac{LK}{2\pi} \quad (5)$$

Where L (0.2 m) is the length of the wire (see Figure 2), and K (m^{-1}) is the wavenumber of the perturbations on the liquid surface. K is equal to $2\pi/\lambda$, and λ (m) is the wavelength, which is representative of the jet spacing (see Figure 2). Note that the wire velocity (1 mm/s) is small enough compared to the carriage velocity (150 mm/s) to make our steady-state assumption valid. Assuming the solution on the wire as a planar liquid layer, K can be calculated from Eq. (6).

$$\sigma^2 - 2\eta K^2\sigma + \left(gK + \frac{\gamma K^3}{\rho} - \frac{\varepsilon_0}{\rho}E_0^2K^2\right)\tanh(K\,h) = 0 \quad (6)$$

where ε_0 (8.85×10^{-12} F/m) is the dielectric permittivity of free space, E_0 (V/m) is the magnitude of the applied electric field outside the liquid, and h (m) is the average liquid thickness. σ is the perturbation growth rate that can be expressed as

$$\sigma = \frac{\gamma h^3}{3\eta}K^2(q^2 - K^2) \quad \text{where } q = \left[\left(\frac{E_0\varepsilon_0}{\gamma}\right)\left(\frac{\partial E}{\partial r_s}\right)\right]^{1/2} \quad (7)$$

here, r_s (m) is the radius of the solution deposited on the wire, $\frac{\partial E}{\partial r_s}$ is the electric field variation from the wire to the liquid surface. $\frac{\partial E}{\partial r_s}$ and E_0 were calculated by the electric field simulation. Values of η and γ were obtained from experimental measurements, and the gravity effect was neglected for simplicity.

The electric field parameters and solution properties also affect the average velocity (u) and radius (r) of a single jet along the stable cone-jet mode. However, developing a simple analytical formula to relate the jet radius and velocity variation with solution properties is rather complex. The available simplified models are not robust and do not provide a good estimation of the jet radius and velocity. Therefore, researchers usually use simulation or dimensional analysis to estimate these two parameters[35,36]. Regarding the dimensional analysis, the clearest trend can be derived from the experimental data and dimensional analysis introduced in [29,30,37];

$$u \propto \frac{\varepsilon_r\varepsilon_0 E\varsigma}{\eta} \quad (8)$$

$$r \propto \left(\frac{\eta}{\gamma}\right)^{1/2} \quad (9)$$

where ε_r is the relative permittivity (or dielectric constant) of the fluid, ς (V)is the electrostatic potential on the liquid surface, and E (V/m)is the electric field on the surface of the fiber. ε_r is extracted from experimental measurements (available in supporting information file), while ς and E were derived from electric field simulation results.

The theoretical prediction of the density (ρ) was performed based on the mixture theory formula[38]:

$$\rho_{mix} = \phi_{PUR}\rho_{PUR} + \phi_{additive}\rho_{additive} + (1 - \phi_{PUR} - \phi_{additive})\rho_{DMF} \quad (10)$$

where ϕ is the volume fraction.

3.3. Electrostatic physics-based computational model

The static electric field inside the solution deposited on the wire, was calculated based on Maxwell equations ((11) and (12)), where ρ_e (C/m^3)is the space charge density. Moreover, charge movement inside the solution was calculated based on convection-diffusion equations. Finite element modeling was used to solve the governing equations. A two-

dimensional model was developed in COMSOL Multiphysics (version 5.4a) in order to calculate the static electric field and charge distribution inside the solution. The geometrical dimensions of the model were defined similarly as in the experimental setup with an electrode distance of 25cm. The average thickness of the entrained solution on the wire electrode was considered as $h = 0.34\, r_{wire}$ based on aforementioned capillary number.

Voltages of V=+60kV with ρ_e=6×10^{-4} mol/m^3 and V=-10kV with ρ_e=0 mol/m^3 were applied on the two electrodes separately as boundary conditions. To solve these equations, the electrostatics module and transport of diluted species modules were solved together as a stationary problem. Appropriate grids were built based on a grid sensitivity analysis. The tolerances for convergence were selected based on sensitivity analysis in such a way that a further increase in the tolerance did not change the results anymore (changes were below 5%).

$$\boldsymbol{E} = -\nabla V \tag{11}$$

$$\nabla.(\varepsilon_0 \varepsilon_r \boldsymbol{E}) = \rho_e \tag{12}$$

4. Results

4.1. Solution characterization

According to the aforementioned mathematical models and literature [39], for the constant operating conditions, solution properties are the primordial parameters influencing the electrospinning process and its throughput. These properties include the polymer chemistry and solvents used, concentration, conductivity, surface tension, and relative permittivity of the solvents. All these parameters were measured experimentally and used as inputs to our mathematical models. The influence of these parameters on solution entrainment on the wire electrode as well as the cone-jet formation was investigated in this study. The focus has been set on the effect of spinning solution additives, and therefore the polymer (PUR), the concentration (14.5 % w/v), the solvent (DMF), and the electrospinning parameters were kept constant throughout the whole set of experiments. Additives have been selected in the class of polydimethylsiloxane-based polymers due to the frequent use of silicon-based materials as lubricants in the polyurethane industry, and TEAB was used as a comparison point, as salts were often added to optimize spinning conditions by increasing the conductivity of the solution[40]. The results of the solution characterization will be discussed in the following paragraphs. It is noteworthy that the emulsions prepared were heterogeneous (see Figure S2 in the supporting information) and that the measured solution properties do not refer to the bulk solution properties.

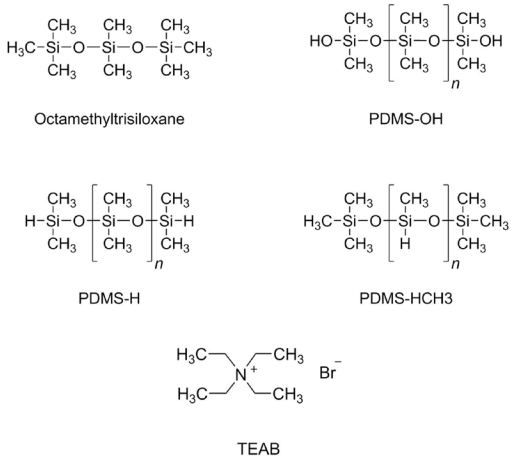

Scheme 1 Chemical structure of the additives used in PUR-DMF electrospinning solutions.

4.1.1.Surface tension

The addition of polyurethane to DMF did not significantly change the surface tension with respect to the pure solvent. When adding 2% w/w of PDMS-OH with respect to the polymer, a large drop in the surface tension was observed (from 35.43to 21.5 mN/m), related to the formation of an emulsion (Figure 3). Further addition of PDMS-OH, up to 20% w/w, only decreased the measured value slightly down to 20.8 mN/m. High molecular weight PDMS-OH and PDMS-H also resulted in a significant drop of the surface tension (25.6 and 23.2 mN/m, respectively). PDMS-HCH_3 and octamethyltrisiloxane had a smaller effect on the solution property (29.9 and 35.1 mN/m, respectively). These values are explained by the fact that the first three additives are not miscible with DMF, therefore forming an emulsion and concentrating at the surface of the solution because of their smaller surface energy as compared to the solvent. On the other hand, the addition of TEAB did not significantly affect the surface tension of the spinning solutions.

4.1.2.Electrode wettability and solution entrainment

In the electrospinning setup used for this work, the spinning electrode is made of a steel wire. Therefore, in order to better understand the influence of the solution properties on the wetting behavior and entrainment of the spinning solutions on the wire electrode, a model system was used. The polymer solution's contact angle on a flat steel plate was recorded with a drop shape analyzer. Without additive, the contact angle of PUR-DMF was 44.3 ± 0.7°. When adding PDMS additives, all the solutions had better wetting properties on steel, thus lower contact angles. Increasing the amount of PDMS-OH further decreased the contact angle, down to 29.0 ± 0.8° at 20 % w/w (Table S1 in the supporting information file). The addition of TEAB, on the other hand, had a small influence on steel wettability. Based on our theoretical calculations, adding PDMS additives resulted in higher solution entrainment on the wire and the solution film thickness increases, which is in alignment with our experimental observations.

4.1.3.Conductivity

The electrical conductivity of PUR-PDMS solutions was independent of the additive concentration and of the PDMS type. The conductivity of all tested solutions was between 0.597 and 0.977 µS/cm, whereas pure DMF had a conductivity of 0.342 µS/cm (See Table S1 in the supporting information file). When TEAB salt was added in a small amount (0.2 % w/w) to PUR solutions, the solution conductivity logically increased to 64.26 µS/cm.

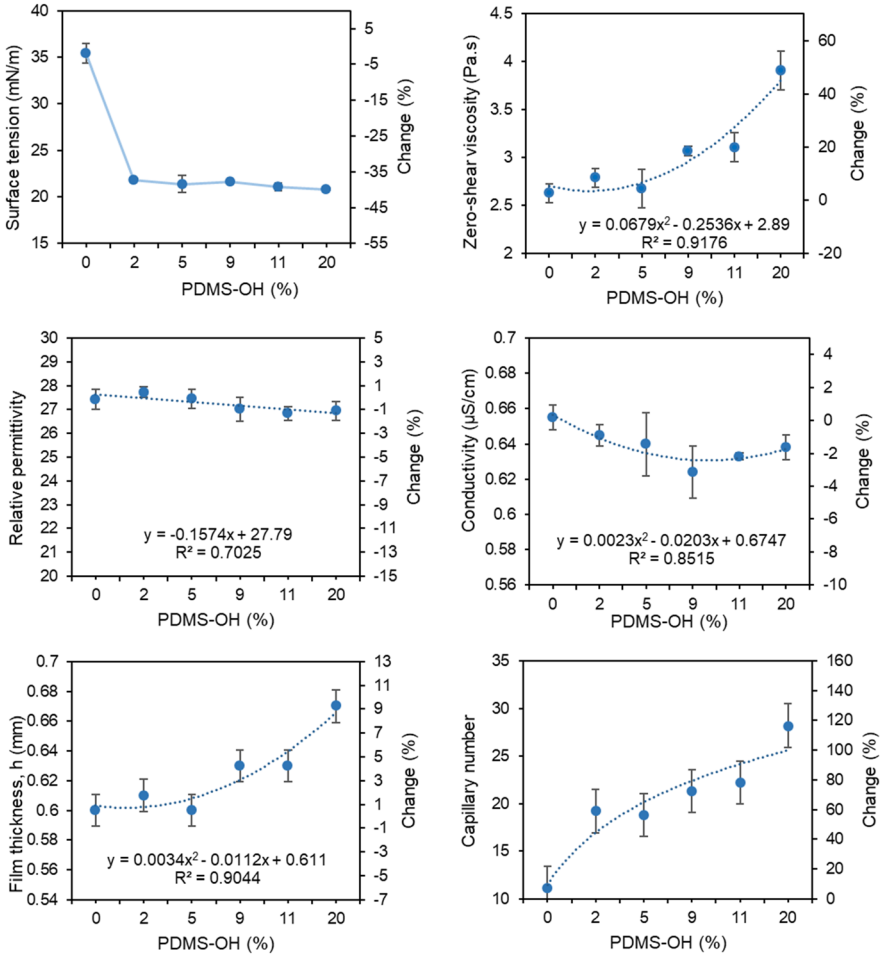

Figure 3 Variation of the solution properties with the addition of PDMS-OH; a) surface tension, b) viscosity, c) average relative permittivity for applied frequencies between 200 to 20000 (MHz), d) conductivity, e) average film thickness on the wire (theoretical calculation), f) Capillary number (theoretical calculation).

4.1.4.Rheological properties

In order to understand the influence of the solution rheological properties on the electrospinning behavior, flow curves were recorded on a rotational rheometer. Very similar behavior was observed for all measured solutions, following a Newtonian behavior at the low shear rate and displaying typical shear-thinning while increasing $\dot{\gamma}$ (Figure S3 in supporting information). All solutions containing polysiloxane additives exhibit slightly higher η_0 than the reference solution without additive (2.79 to 3.33 Pa.s versus 2.63 Pa.s for the pure polyurethane solution). On the other hand, the solution with 0.2 % TEAB has lower viscosity at all shear rates, following the same shear-thinning behavior. Accordingly, these results show that no strong intermolecular interactions exist between PUR and the used additives in DMF solutions. Figure 3 shows that viscosity has the highest impact on the amount of the solution deposited on the wire by the carriage.

4.1.5.Relative permittivity

The relative permittivity of the solutions was measured using the OCP method with the DAK 3.5 probe system in order to assess the influence of the PDMS-OH additive on the dielectric constant of the solution. As the relative permittivity is frequency-dependent, we used the average value of relative permittivity for low frequencies (200 to 1000 MHz) for our calculations to be close to the response of the medium to static electric fields (i.e., low frequency and/or DC mode). As depicted in Figure 3, the relative permittivity did not change significantly when the PDMS-OH additives were added,

thus not impacting the capacity of the solutions for polarization with the electric field. This positive effect will be discussed in the following sections.

4.2. Electrospun fiber characterization

4.2.1. Water contact angle of the membranes

In order to study the effect of additives on the macroscopic and physical properties of the resulting electrospun membranes, the water contact angle was measured. The water drop had a contact angle of 129.3° on a membrane made from simple PUR-DMF solution. As shown in Table 1, the addition of PDMS additives had no effect on the wettability with water. All membranes containing polysiloxane additives had similar values of 128.0 to 131.5° with small standard deviations. Similarly, the concentration of PDMS-OH in the spinning solution did not change the resulting contact angle from 2 % to 20 % of the additive. However, the addition of TEAB reduced this value significantly to 96.9°, which can be attributed to the ionic character of the salt, increasing the hydrophilicity and, therefore, the wettability of the membrane.

Table 1 Electrospinning process throughput, the water contact angle of polyurethane membranes, the respective mean fibers diameter, and estimated number of jets as a function of additives.

Additive	Throughput (g/cm^2)	Water contact angle (°)	Mean fiber diameter (nm)	Estimated number of jets***
-	0.99 *	129.3 ± 1.5	265 ± 87	16
2 % PDMS-OH	5.55 ± 0.39	129.0 ± 0.9	258 ± 153	29
5 % PDMS-OH	6.09 ± 0.32	128.0 ± 1.4	218 ± 112	29
9 % PDMS-OH	6.26 ± 0.38	131.5 ± 0.4	268 ± 184	29
11 % PDMS-OH	6.31 ± 0.69	130.8 ± 1.2	302 ± 155	29
20 % PDMS-OH	6.54 ± 0.37	130.3 ± 1.4	253 ± 102	32
2 % octamethyltrisiloxane	4.66 ± 0.42	129.1 ± 1.8	241 ± 112**	-
2 % PDMS-H	5.73 ± 0.72	129.5 ± 0.8	236 ± 114**	-
2 % PDMS-HCH3	5.84 ± 0.58	129.4 ± 2.1	267 ± 103	-
2 % high MW PDMS-OH	6.57 ± 0.49	128.7 ± 1.3	234 ± 126**	-
0.2 % TEAB	0.69 *	96.9 ± 5.1	191 ± 62	-

* Inhomogeneous membrane surfaces were obtained

** Beads were formed together with fibers and ignored for the mean diameter determination

*** Theoretical calculations for a wire with 200mm length, as employed in our experimental setup

4.2.2. Fiber diameter and morphology

The mean fiber diameter of membranes obtained from PUR-PDMS-OH solutions was also not affected by the amount of additive. The values stayed constant around 250 nm within the concentration range tested. As compared with the solution without additive, the fiber size distribution was slightly broader. Octamethyltrisiloxane, PDMS-H, and high MW PDMS-OH also did not affect the arithmetic mean fiber diameter but induced the formation of beads, which are considered as defects with regard to membrane homogeneity. PDMS-HCH_3, on the other side, was behaving as

PDMS-OH and did not influence the membrane morphology at 2 % concentration. The addition of TEAB salt to the spinning solution significantly reduced the fiber diameter, producing bimodal fiber size distribution because of the increased solution conductivity[40]. Scanning electron micrographs pictures of the electrospun membranes are available in the supporting information file.

4.2.3. Fiber surface chemistry

The surface elemental composition of electrospun fibers was analyzed by XPS. As expected, increasing amounts of PDMS-OH in the fibers resulted in the increased atomic concentration of oxygen and silicon atoms on the fibers' surface. However, the silicon concentration at 20% PDMS-OH was almost the same value as for pure PDMS. Theoretical values for surface Si concentration were calculated considering a homogeneous blend of additive and polyurethane and 25 % Si content in pure PDMS. It is noteworthy that pure polyurethane contains a small amount of silicon arising from lubricants added by the manufacturer (3.82 % Si). The results show that in the nanofibers, the experimental atomic surface concentration of silicon is much higher (> 3-fold) than the calculations (Table S3 of the supporting information file). This indicates an enriched additive concentration at the surface of the fibers, also highlighted by the large decrease in nitrogen atoms concentration, being selective for the PUR polymer, at the surface.

4.3. Impact of solution properties on cone-jet formation

The influence of the solution properties on cone-jet formation is investigated in this section. Applying a strong electric field to the entrained solution forms undulations, or so-called Taylor cones, due to the accumulation of charge in the fluid and the resultant competition between surface tension and surface charge repulsion. Increasing the electric field strength leads to a higher accumulation of the surface charges on the cones. As a result, these cones become unstable and develop charged viscoelastic jetting from the tips of the cones. The electric forces originating from the charges at the surface of the electrospinning jet cause the solution to stretch and form the nanofibers. The aforementioned solution properties affect the number and shape of the cones as well as the radius and velocity of the jets. We calculated the number of jets based on the theoretical relations presented in section 3.2. The addition of 2 % w/w PDMS-OH significantly increased the number of jets on the electrode wire (**Table 1**). This can be attributed to the significant change in the surface tension due to the addition of PDMS-OH (Figure 3). Physically, this finding implies that by lowering the surface tension, the liquid solution has less resistive forces to overcome to form a jet as the fluid is held together less tightly.

It is expected that any change in the solution's conductivity modifies the surface charges and affects the cone shape and cone-jet formation dynamics. As such, the cone volume increases and the cone shape becomes steeper with increasing solution conductivity [37,41]. The increased charge carried by the jets results in higher electric forces; thus, a narrower initial jet and less mass transported [41]. A benefit of adding PDMS-OH is that it increases the number of the jets due to reducing the surface tension while it does not decrease the volume and throughput of the cones as the conductivity and surface charge density (SCD) remain almost constant (or even slightly decreases the conductivity, hence increasing the SCD). On the other hand, for the stable cone-jet spinning mode, the velocity and diameter of the jets increase due to the changes in the surface tension, viscosity, and deposited solution on the wire electrode (see section 3.2). In order to evaluate these hypotheses, we investigated in the next paragraph the amount of the formed jets on the wire based on theoretical calculations and experimental observations.

4.3.1. Jet density calculation and validation

The results of the theoretical calculations and experimental observations of the jet density (i.e., number of jets per unit length of wire) are shown in Figure 4. Experimental observation shows that for the solution with only 2% PDMS-OH, the jet density increased more than two times compared to the solution without additives (i.e., 60±6 (1/m) vs. 125±13 (1/m)). The theoretical model could predict the jet densities very well, and the difference between theoretical calculations and experimental observations was not significant, $t(5) = 0.56$, $p > .05$.

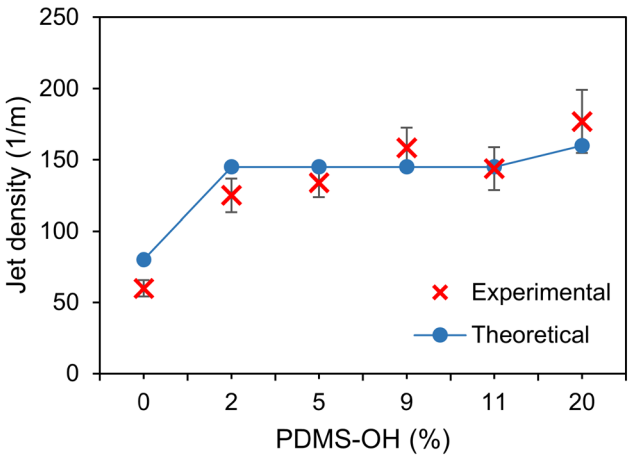

Figure 4 Experimental observations and theoretical calculation of the number of jets per unit length of wire as a function of the amount of PDMS-OH.

In order to validate these hypotheses, videos of the electrospinning process in the instrument chamber were recorded. As shown in Figure 5, the solution containing PDMS-OH additive directly formed a textured film around the wire electrode, and the first jet appeared after less than 100 ms. After around 500 ms, jets were formed at almost equal distances on the whole lengths of the recorded segment of the electrode (35 mm).

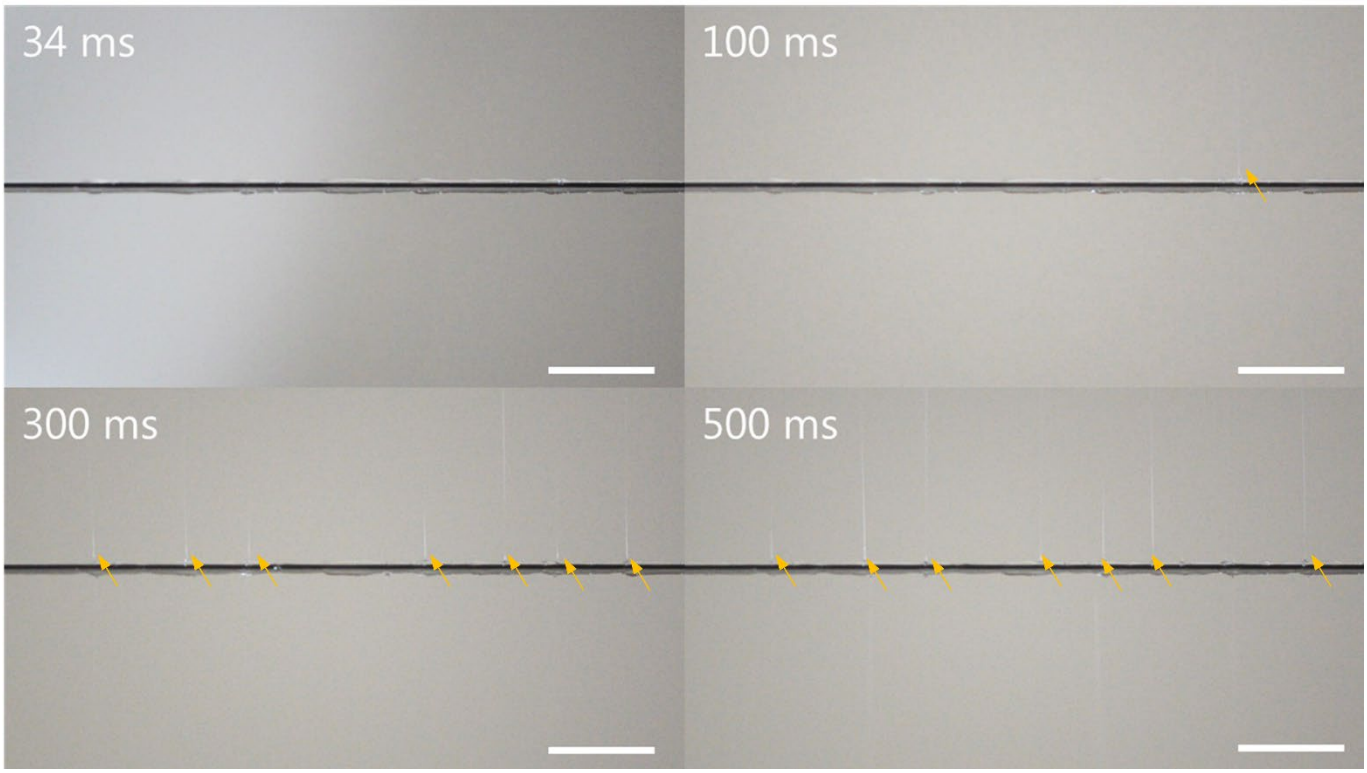

Figure 5 Pictures of the electrospinning process of a PUR solution in DMF containing 2% PDMS-OH additive. The horizontal black line in the center of each frame is the steel wire electrode. Scale bars represent 5 mm.

By contrast, the PUR solution in DMF without additives (Figure 6) appeared to form a smoother film around the wire electrode due to the higher surface tension as expected by the Capillary number (Figure 3). In this case, the first jets only formed after around 300 ms. After 500 ms, only very few jets were visible. Moreover, some jets briefly formed and disappeared, as highlighted by the white circle (Figure 6, lower-left frame). The recorded segment of the electrode is 32 mm.

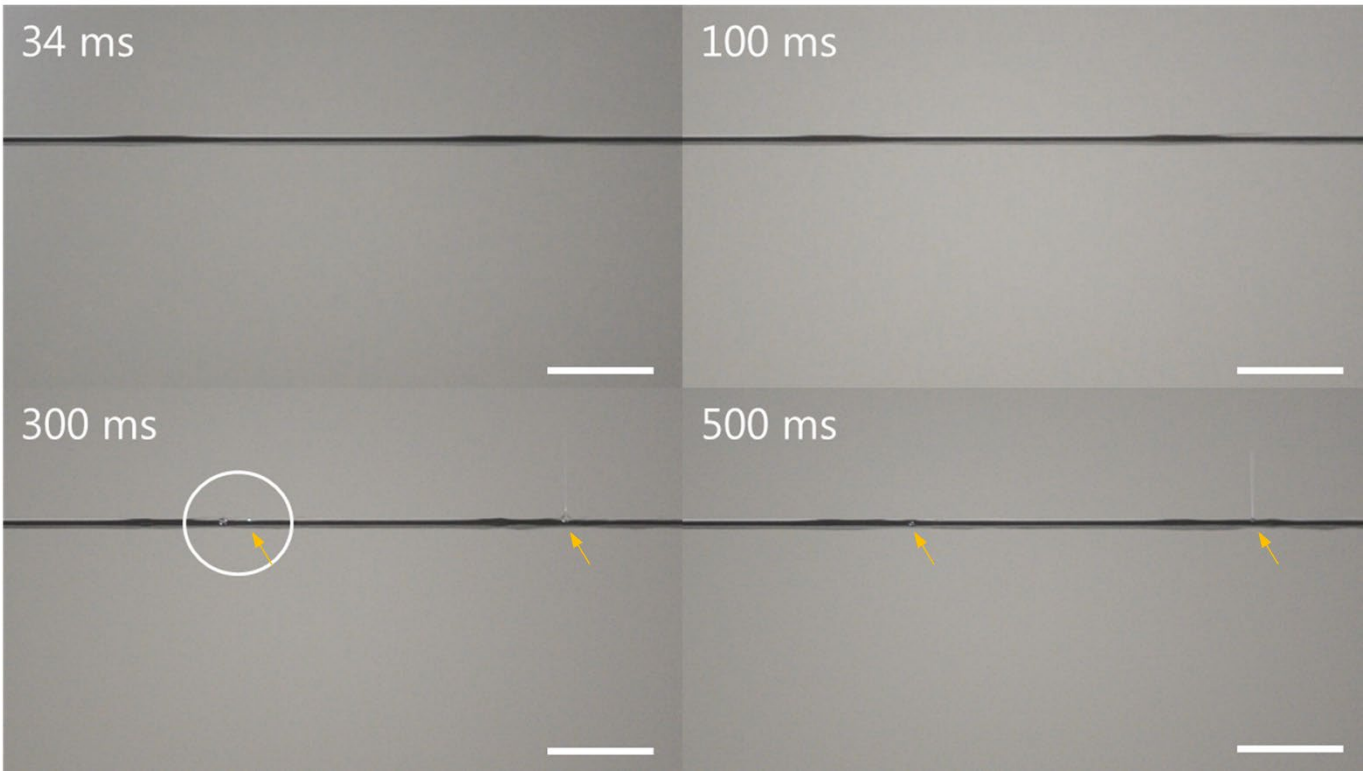

Figure 6 Pictures of the electrospinning process of a PUR solution in DMF without additives. The horizontal black line in the center of each frame is the steel wire electrode. Scale bars represent 5 mm.

4.4. Impact of solution properties on the electrospinning throughput

We quantify the impact of solution properties on the electrospinning throughput. To this end, electrospinning of nanofibers was performed with constant collecting substrate speed for all samples. Membranes were then cut with accuracy using a punching machine and weighed on a microbalance to determine the throughput of the process as membrane weight per area. Since the baking paper speed (i.e., collecting substrate rewinding speed) and the measured area were fixed constant to 18 mm/min and 1 cm^2, the throughput in weight per area per time (g/cm^2 min) is mathematically computable for comparison purposes in the future studies. As shown in Figure 7a, the addition of PDMS-OH to polyurethane solutions leads to a steep increase of the electrospinning throughput, but further increasing the concentration of PDMS-OH does not increase the throughput further. This shows that concentration is not the main driving force here. Figure 7b shows the variation of the most important parameters contributing to the throughput (see Eq. (4)).

Figure 7a shows that with as low as 2% w/w additive, the membrane weight increased from 0.99 to 5.55 g/cm^2 before reaching a plateau between 5.55 g/cm^2 and 6.54 g/cm^2 for 2% and 20% w/w PDMS-OH, respectively (Figure 7). This rapid increase in throughput is well-demonstrated in Figure 7b too. Adding a 2% w/w additive reduces the jet velocity by 6% but increases the jet number and jet radius by 81% and 31%, respectively. Although we cannot assume a linear superposition effect for these parameters, the numbers shed light on the underlying physics of the experimentally observed increase in the throughput as a function of the additives. Increasing the additive from 2% to 20% w/w does

not increase the throughput significantly. This plateau-shape behavior can also be interpreted by Figure 7b. By increasing the additive from 2% to 20% w/w, the jet velocity highly decreases (negative impact on throughput), while the number and radius of the jets increase with a lower rate.

This trend was verified with the other PDMS-based additives, where (Figure 7). Contrarily, solutions of higher conductivity containing TEAB as an additive led to a lower or comparable electrospinning throughput than the pristine solution. As such, adding TEAB to the solution did not decrease the surface tension (Table 1), so the number of the jets did not increase, and on the other hand, by increasing the conductivity (Table 1), SCD decreased, which led to smaller cones. As a result, we observed lower throughput. The same logic could be applied to interpret the throughput enhancement due to other additives. These experimental observations verify our theoretical predictions presented in the previous section.

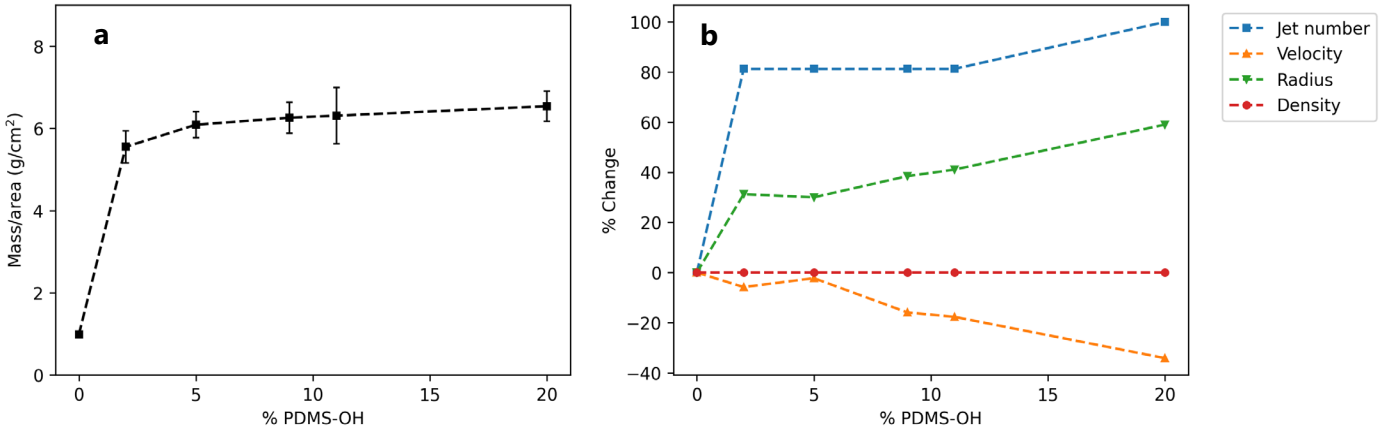

Figure 7 Effect of PDMS-OH additives on throughput; a) Weight per area of electrospun membranes as a function of the amount of PDMS-OH additive (experimental data), b) percentage of variation of the parameters contributing to throughput (i.e., jet number, average jet velocity, average jet radius, and solution density) as a function of the amount of PDMS-OH (mathematical calculation).

5. Discussion

Polydimethylsiloxanes are polymers of low polarity and low surface tension, typically below 20 mN/m. During the wire-based electrospinning process, the polymer solution is coated on a metal wire, which acts as the spinning electrode. When PDMS additives are present, they diffuse to the surface of the liquid polymer film and reduce the total surface tension of the spinning solution. This allows an easier deformation of the surface upon application of the electric potential, which in turn allows the electrical charges to locally accumulate and initiate jet formation through the build-up of Taylor cones. This hypothesis is supported by theoretical evaluations and XPS surface elemental measurements, which showed a large increase of silicon atoms on the surface of the nanofibers with increasing PDMS amount, indicating surface enrichment in PDMS.

Additionally, the throughput is also determined by the lifetime of the jets formed on the electrode. As previously reported in the literature, jet stability and lifetime are mostly dictated by the solution's viscoelastic properties. For instance, Deshawar and Chokshi [42] showed that increasing polymer concentration or fluid elasticity resulted in suppression of jet instabilities, leading to the production of more homogeneous fibers. Therefore, the slight viscosity increase, which results from the addition of PDMS additives, is beneficial in maintaining long-lasting jets and achieving higher throughputs. Moreover, as seen in the results, the addition of PDMS additives affects the velocity, diameter, and the number of the jets due to the modification of the surface tension, viscosity, and the amount of solution entrained on the wire electrode.

Taken together, these results confirm that jet formation and stability are two important parameters for the electrospinning throughput, and hence for the profitability of the process. This study shows that the addition of PDMS-

based surfactants lowers the surface tension and increases the wettability of the polyurethane-DMF solution, which in turn improves the electrospinnability by facilitating the formation of jets.

It has been previously shown that the electrospinnability of PUR can be influenced by the addition of salt to the polymer solution [21]. However, higher conductivity always leads to a decrease in cone size and fiber average diameter and, therefore, a change in membrane properties such as tensile strength or total surface area. In this work, it was successfully demonstrated that the electrospinning efficiency of PUR solutions could also be improved by the use of PDMS-based additives without affecting the membrane properties simply by modifying the rheological properties of the electrospinning solution.

6. Conclusion

The impact of silicon-based additives in the electrospinning of polyurethane solutions using a needleless setup was investigated to gain insights into the main factors influencing the process throughput. A joint experimental-theoretical study was performed, and it was observed that among all the solutions properties examined, the surface tension and the viscosity had the greatest impact. Using XPS, we observed a large concentration of Si atoms at the surface of the fibers, and video recording of the electrospinning process allowed us to relate the jet formation and lifetime to the solution properties. We showed that PDMS-based additives increase the electrospinning rate by decreasing the surface tension, thus easing the jet formation and increasing the viscosity leading to more jet stability and lifetime. Increasing the viscosity also increased the solution film thickness on the wire electrode, so the maximal amount of solution that is available for electrospinning.

Based on these results, additives that decrease the surface tension and conductivity of the solutions while increasing their viscosity should be used to achieve higher throughput in DMF-based spinning solutions. We demonstrated that a higher throughput was achieved with our needless electrospinning setup for concentrations of PDMS-OH higher than 2 wt% added to the pristine solution. Therefore, industrial applications using electrospinning of PUR, such as high-performance filters, wound dressing materials, or protective textiles, for example, could largely benefit from this technique for reducing the costs of material production by saving processing time. Further experiments are needed to identify the impact of the additives on other spinning solutions which are not DMF-based or with different polymers. In this regard, further studies are ongoing in our laboratory to enlarge the scope of applications. Moreover, further experiments are needed to study whether changing the process parameters such as the speed of the carriage or the size of the orifice dispensing the solution on the wire could lead to a larger throughput in wire-based electrospinning.

■ ASSOCIATED CONTENT

- **Supporting Information:** Additional experimental details, materials and characterization, modeling approach, and figures including additional photographs, SEM micrographs, jet number calculation, and optical measurements

Author Contributions: Conceptualization: N.L., R.R. and G.F.; methodology: N.L, K.I, J.S., M.C., G.F, T.D, and R.R..; experiments: N.L J.S, K.I., M.C., and S.H.; theoretical and computational model: K.I, and T.D..; writing—original draft preparation: K.I, N.L, and J.S..; writing—review and editing: all the authors; supervision, R.R.; project administration, R.R., and N.L; funding acquisition, R.R. and G.F. All authors have read and agreed to the published version of the manuscript.

Conflicts of Interest: The authors declare no conflict of interest. The funders had no role in the design of the study, in the collection, analyses, or interpretation of data, in the writing of the manuscript, or in the decision to publish the results.

Acknowledgment: The authors would like to acknowledge the CCMX Materials Challenge "Self-Care Materials" for funding this project.

In Memoriam: The authors would like to dedicate this paper to the memory of our dear colleague Dr. Giuseppino Fortunato, who passed away while this paper was being written.

7. Data availability

The raw/processed data required to reproduce these findings cannot be shared at this time due to legal or ethical reasons.

8. References

(1) Sill, T. J.; von Recum, H. A. Electrospinning: Applications in Drug Delivery and Tissue Engineering. *Biomaterials*. Elsevier May 1, 2008, pp 1989–2006.

(2) Vellayappan, M. V.; Venugopal, J. R.; Ramakrishna, S.; Ray, S.; Ismail, A. F.; Mandal, M.; Manikandan, A.; Seal, S.; Jaganathan, S. K. Electrospinning Applications from Diagnosis to Treatment of Diabetes. *RSC Advances*. Royal Society of Chemistry September 5, 2016, pp 83638–83655.

(3) Agarwal, S.; Wendorff, J. H.; Greiner, A. Use of Electrospinning Technique for Biomedical Applications. *Polymer*. Elsevier BV December 8, 2008, pp 5603–5621.

(4) Persano, L.; Camposeo, A.; Tekmen, C.; Pisignano, D. Industrial Upscaling of Electrospinning and Applications of Polymer Nanofibers: A Review. *Macromol. Mater. Eng.* **2013**, *298* (5), 504–520.

(5) Angammana, C. J.; Jayaram, S. H. Fundamentals of Electrospinning and Processing Technologies. *Part. Sci. Technol.* **2016**, *34* (1), 72–82.

(6) Forward, K. M.; Rutledge, G. C. Free Surface Electrospinning from a Wire Electrode. *Chem. Eng. J.* **2012**, *183*, 492–503.

(7) Döpke, C.; Grothe, T.; Steblinski, P.; Klöcker, M.; Sabantina, L.; Kosmalska, D.; Blachowicz, T.; Ehrmann, A. Magnetic Nanofiber Mats for Data Storage and Transfer. *Nanomaterials* **2019**, *9* (1), 92.

(8) Greiner, A.; Wendorff, J. H. Electrospinning: A Fascinating Method for the Preparation of Ultrathin Fibers. *Angew. Chemie Int. Ed.* **2007**, *46* (30), 5670–5703.

(9) Haider, A.; Haider, S.; Kang, I.-K. A Comprehensive Review Summarizing the Effect of Electrospinning Parameters and Potential Applications of Nanofibers in Biomedical and Biotechnology. *Arab. J. Chem.* **2018**, *11* (8), 1165–1188.

(10) Tao, J.; Shivkumar, S. Molecular Weight Dependent Structural Regimes during the Electrospinning of PVA. *Mater. Lett.* **2007**, *61* (11–12), 2325–2328.

(11) Zeng, J.; Haoqing, H.; Schaper, A.; Wendorff, J. H.; Greiner, A. Poly-L-Lactide Nanofibers by Electrospinning – Influence of Solution Viscosity and Electrical Conductivity on Fiber Diameter and Fiber Morphology. *e-Polymers* **2003**, *3* (1).

(12) Son, W. K.; Youk, J. H.; Lee, T. S.; Park, W. H. The Effects of Solution Properties and Polyelectrolyte on Electrospinning of Ultrafine Poly(Ethylene Oxide) Fibers. *Polymer (Guildf).* **2004**, *45* (9), 2959–2966.

(13) Tan, S.-H.; Inai, R.; Kotaki, M.; Ramakrishna, S. Systematic Parameter Study for Ultra-Fine Fiber Fabrication via Electrospinning Process. *Polymer (Guildf).* **2005**, *46* (16), 6128–6134.

(14) Pelipenko, J.; Kristl, J.; Janković, B.; Baumgartner, S.; Kocbek, P. The Impact of Relative Humidity during Electrospinning on the Morphology and Mechanical Properties of Nanofibers. *Int. J. Pharm.* **2013**, *456* (1), 125–134.

(15) Yazgan, G.; Dmitriev, R. I.; Tyagi, V.; Jenkins, J.; Rotaru, G.-M.; Rottmar, M.; Rossi, R. M.; Toncelli, C.; Papkovsky, D. B.; Maniura-Weber, K.; Fortunato, G. Steering Surface Topographies of Electrospun Fibers: Understanding the Mechanisms. *Sci. Rep.* **2017**, *7* (1), 158.

(16) Yazgan, G.; Popa, A. M.; Rossi, R. M.; Maniura-Weber, K.; Puigmartí-Luis, J.; Crespy, D.; Fortunato, G. Tunable Release of Hydrophilic Compounds from Hydrophobic Nanostructured Fibers Prepared by Emulsion Electrospinning. *Polymer (Guildf).* **2015**, *66*, 268–276.

(17) Jacobs, V.; Anandjiwala, R. D.; Maaza, M. The Influence of Electrospinning Parameters on the Structural Morphology and Diameter of Electrospun Nanofibers. *J. Appl. Polym. Sci.* **2010**, *115* (5), 3130–3136.

(18) Theron, S. A.; Zussman, E.; Yarin, A. L. Experimental Investigation of the Governing Parameters in the Electrospinning of Polymer Solutions. *Polymer (Guildf).* **2004**, *45* (6), 2017–2030.

(19) Xue, J.; Wu, T.; Dai, Y.; Xia, Y. Electrospinning and Electrospun Nanofibers: Methods, Materials, and Applications. *Chemical Reviews*. American Chemical Society April 24, 2019, pp 5298–5415.

(20) Luo, C. J.; Stoyanov, S. D.; Stride, E.; Pelan, E.; Edirisinghe, M. Electrospinning versus Fibre Production Methods: From Specifics to Technological Convergence. *Chem. Soc. Rev.* **2012**, *41* (13), 4708.

(21) Cengiz, F.; Jirsak, O. The Effect of Salt on the Roller Electrospinning of Polyurethane Nanofibers. *Fibers Polym.* **2009**, *10* (2), 177–184.

(22) Thoppey, N. M.; Bochinski, J. R.; Clarke, L. I.; Gorga, R. E. Unconfined Fluid Electrospun into High Quality Nanofibers from a Plate Edge. *Polymer (Guildf).* **2010**, *51* (21), 4928–4936.

(23) Kim, H. Y. *Electronic Spinning Apparatus, and a Process of Preparing Nonwoven Fabric Using the Same*; US 7,332,050 B2; U.S. Patent, 2008.

(24) Ding, Y.; Hou, H.; Zhao, Y.; Zhu, Z.; Fong, H. Electrospun Polyimide Nanofibers and Their Applications. *Prog. Polym. Sci.* **2016**, *61*, 67–103.

(25) Kaatze, U.; Góttmann, O.; Podbielski, R.; Pottel, R.; Terveer, U. *Dielectric Relaxation in Aqueous Solutions of Some Oxygen-Containing Linear Hydrocarbon Polymers*; 1978; Vol. 82.

(26) Ellison, W. J. Permittivity of Pure Water, at Standard Atmospheric Pressure, over the Frequency Range 0–25THz and the Temperature Range 0–100°C. *J. Phys. Chem. Ref. Data* **2007**, *36* (1), 1–18.

(27) Gregory, A. P.; Clarke, R. N. Dielectric Metrology with Coaxial Sensors. *Meas. Sci. Technol.* **2007**, *18* (5), 1372–1386.

(28) R Core Team. R: A Language and Environment for Statistical Computing. Vienna, Austria 2021.

(29) Higuera, F. J. Flow Rate and Electric Current Emitted by a Taylor Cone. *J. Fluid Mech.* **2003**, *484* (484), 303–327.

(30) Gañán-Calvo, A. M. On the General Scaling Theory for Electrospraying. *J. Fluid Mech.* **2004**, *507* (507), 203–212.

(31) Quéré, D. Fluid Coating on a Fiber. *Annu. Rev. Fluid Mech.* **1999**, *31* (1), 347–384.

(32) Rogers, J. T. Laminar Falling Film Flow and Heat Transfer Characteristics on Horizontal Tubes. *Can. J. Chem. Eng.* **1981**, *59* (2), 213–222.

(33) Thoppey, N. M.; Gorga, R. E.; Bochinski, J. R.; Clarke, L. I. Effect of Solution Parameters on Spontaneous Jet Formation and Throughput in Edge Electrospinning from a Fluid-Filled Bowl. *Macromolecules* **2012**, *45* (16), 6527–6537.

(34) Miloh, T.; Spivak, B.; Yarin, A. L. Needleless Electrospinning: Electrically Driven Instability and Multiple Jetting from the Free Surface of a Spherical Liquid Layer. *J. Appl. Phys.* **2009**, *106* (11).

(35) Zheng, Y.; Xin, B.; Li, M. Model Development and Validation of Electrospun Jet Formation. *Text. Res. J.* **2019**, *89* (11), 2177–2186.

(36) Nezbeda, I.; Jirsák, J.; Moučka, F. Molecular Modeling and Simulations. *Electrospun Nanofibers* **2017**, 255–275.

(37) Wang, C.; Hsu, C. H.; Lin, J. H. Scaling Laws in Electrospinning of Polystyrene Solutions. *Macromolecules* **2006**, *39* (22), 7662–7672.

(38) Sarkar, J.; Ghosh, P.; Adil, A. A Review on Hybrid Nanofluids: Recent Research, Development and Applications. *Renew. Sustain. Energy Rev.* **2015**, *43*, 164–177.

(39) Li, Z.; Wang, C. Effects of Working Parameters on Electrospinning. In *One-Dimensional nanostructures*; 2013; pp 15–28.

(40) Angammana, C. J.; Jayaram, S. H. Analysis of the Effects of Solution Conductivity on Electro-Spinning Process and Fiber Morphology. In *2008 IEEE Industry Applications Society Annual Meeting*; IEEE, 2008; pp 1–4.

(41) Stanger, J.; Tucker, N.; Kirwan, K.; Staiger, M. P. Effect of Charge Density on the Taylor Cone in Electrospinning. *Int. J. Mod. Phys. B* **2009**, *23* (6–7), 1956–1961.

(42) Deshawar, D.; Chokshi, P. Stability Analysis of an Electrospinning Jet of Polymeric Fluids. *Polymer (Guildf).* **2017**, *131*, 34–49.

Table of Contents/Abstract Graphics

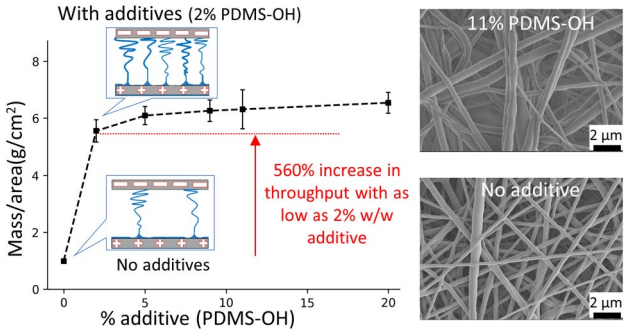

Figure ToC1 For Table of Contents Only